Progress In Electromagnetics Research C, Vol. 52, 83–92, 2014

Analysis of CPW-Fed UWB Antenna for WiMAX and WLAN Band Rejection

Sarah Jacob*, Arimpoorpallan O. Lindo, Chakkanattu M. Nijas, Chandroth K. Aanandan, and Pezholil Mohanan

Abstract—A compact ultra wide band (UWB) antenna with dual band notch characteristics is proposed. The antenna consists of a coplanar waveguide (CPW) fed bevelled rectangular patch and a modified rectangular ground plane. A Z-shaped meander line parasitic element and a pair of symmetrical L-shaped quarter-wavelength stubs are employed to realise band-notched functions at WiMAX and WLAN bands respectively. By optimizing the dimensions and positions of these notch structures, the desired notch-bands of WLAN and WiMAX are achieved. Unlike other dual band-notched antennas reported in literature this antenna has a merit of regulating the centre frequency as well as the bandwidth of both the notched bands easily and independently. The measured -10 dB S_{11} covers the bandwidth from 2.5 to 11.5 GHz, with two notched bands from 3.3 to 3.6 GHz and 5.2 to 5.75 GHz. The proposed antenna exhibits nearly omni-directional radiation patterns with moderate gain and small group delay variations less than 0.5 ns over the entire operating bandwidth except at the notched bands. Moreover, by using antenna transfer function, the time domain characteristic of the antenna is also studied to confirm its suitability for UWB pulse communication.

1. INTRODUCTION

Ultra wide band (UWB) technology gains a lot of popularity among the wireless industry due to its capability of offering high speed short-range wireless communication with low power spectral density. The high demands on such communication systems have triggered research into many UWB antenna designs. Printed monopole antennas of various shapes and feeding structures have been popular due to their excellent electrical characteristics and other features such as small size, light weight and ease of fabrication. Because of the co-existence of other narrowband wireless services, such as IEEE 802.16 WiMAX (3.3–3.7 GHz), C-band satellite communication systems (3.7–4.2 GHz) and IEEE 802.11a WLAN (5.15–5.825 GHz), an additional requirement for UWB antennas is to reject these bands within the pass band of UWB (3.1–10.6 GHz).

Recently, a number of UWB antennas with band-notched characteristics have been proposed, and the conventional techniques for band-notched design include: cutting slots of different shapes on the radiating patch or in the ground plane [1–6], putting parasitic elements close to the radiator [7–10] and inserting quarter wavelength stubs into the ground plane or in the radiating patch [11–16]. By using these techniques, the centre frequencies of the rejected bands can be adjusted easily by varying the lengths of respective notch structures. However, methods to vary the bandwidth are hardly reported. The major limitations in achieving an efficient dual/ multiple band-notched performances are (1) difficulty in controlling bandwidth of the notch band in a limited space and (2) strong coupling between closely placed band-rejected elements [7]. Moreover, due to the co-existence of several narrow

Received 12 June 2014, Accepted 21 July 2014, Scheduled 24 July 2014

* Corresponding author: Sarah Jacob (sarahjacob12@gmail.com).

The authors are with the Centre for Research in Electromagnetics and Antennas, Department of Electronics, Cochin University of Science & Technology, Cochin-22, Kerala, India.

band wireless services within the pass band of UWB, adjusting the centre frequency as well as the bandwidth of the notched band become significant in UWB communication systems. Many band-notched antenna designs in the literature cannot be adjusted to suit for other avoidable interferences. So, for an efficient band-notched UWB antenna, both the bandwidth and centre frequency of notch band should be controllable. In this paper, a dual band-notched UWB antenna with independently controllable notch characteristics is proposed. Unlike earlier band-notched antenna designs in the literature, this antenna can be adjusted to reject either WiMAX or C-band interferences along with WLAN.

Most of the UWB antenna designs mainly concentrate on two types of feed structures, i.e., microstrip and coplanar waveguide (CPW) line. CPW feed line is preferred because it offers several advantages over conventional microstrip line such as low radiation loss, less dispersion, uniplanar configuration and easy shunt as well as series surface mounting of active and passive devices without via hole [17]. In this paper, a CPW fed UWB monopole antenna employing two compact band-reject elements to realise dual band-notched characteristics is presented. A Z-shaped meander line parasitic element placed in the radiating aperture of the antenna suppresses the radiation at WiMAX band (3.3–3.6 GHz). The meandered structure is actually a microstrip line folded back and forth to lower its resonant frequency with miniaturized size [18]. Thus requires less space for implementation compared to the other designs using parasitic strips that are straight and have length comparable to the radiating aperture. A pair of symmetric L-shaped quarter-wavelength stubs attached to the upper edge of the ground plane eliminates the WLAN band (5.2–5.75 GHz) effectively. The presented approach is very efficient for dual/multiple band-notched design as it has the advantage of controlling both the centre frequency and the bandwidth of the each notched-band independently by adjusting the parameters of the corresponding notch structures. A detailed account of parametric study on notch structures and results are discussed in the following sections.

2. ANTENNA GEOMETRY

Figure 1 shows the geometry of the proposed dual band-notched UWB monopole antenna. It consists of a CPW-fed bevelled rectangular patch and a rectangular ground plane extended to a length L_0+W_1. The extended ground decreases the lower resonance frequency considerably which is clear from comparing Figures 2(a) and 2(b). Rectangular slits ($W_3 \times L_3$) inserted symmetrically on the extended portion of the ground plane, improve performance of the antenna in the lower frequency band further. Bevelling (α_g) of ground plane corners near the feed point enhances the upper edge frequency and also improves the impedance match of the structure appreciably. By incorporating these modifications, an antenna which covers impedance band from 2.5 to more than 12 GHz is obtained as shown in Figure 2. Measured and simulated VSWR of the UWB antenna are shown in Figure 3.

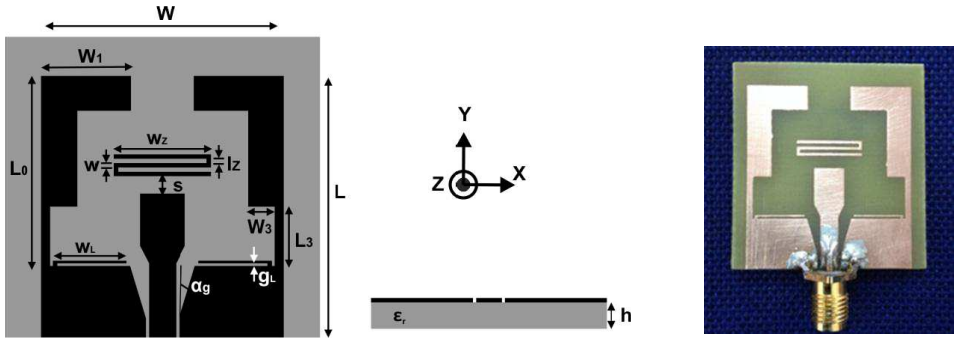

Figure 1. Geometry of the proposed dual band-notched UWB antenna, (a) top view, (b) side view, (c) fabricated antenna. $L\times W\times h = 30\,\text{mm}\times 27\,\text{mm}\times 1.6\,\text{mm}$, $L_0 = 21.8\,\text{mm}$, $W_1 = 10\,\text{mm}$, $L_3 = 6.8\,\text{mm}$, $W_3 = 3\,\text{mm}$, $\alpha g = 16.7°$, $w_Z = 10.8\,\text{mm}$, $l_Z = 0.5\,\text{mm}$, $s = 2\,\text{mm}$, $w = 0.5\,\text{mm}$, $w_L = 8.2\,\text{mm}$, $g_L = 0.3\,\text{mm}$.

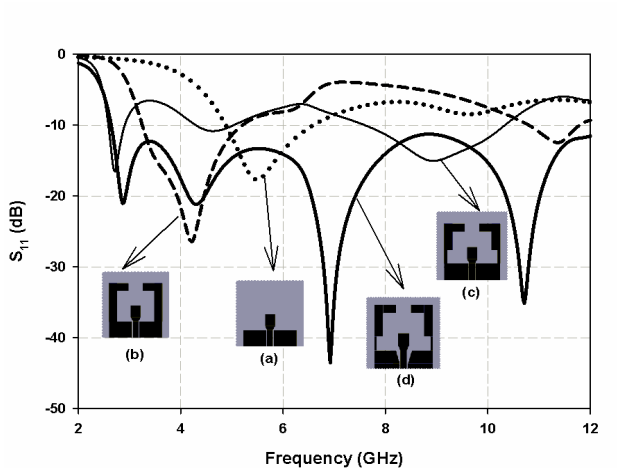

Figure 2. Evolution of the UWB antenna.

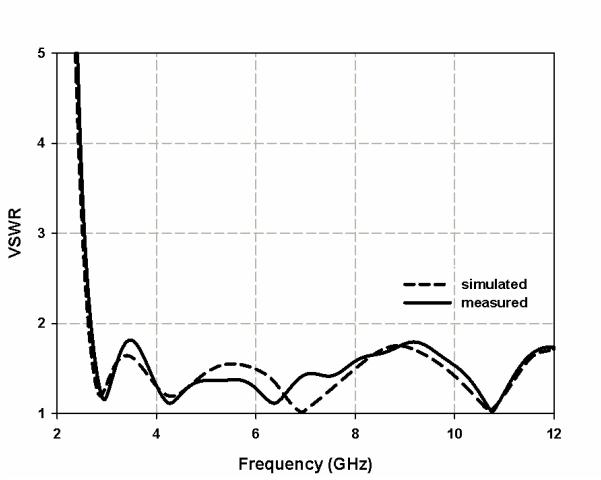

Figure 3. Measured and simulated VSWR of the UWB antenna.

To realise single band-notched function at WiMAX band, a Z-shaped meander line parasitic element is etched at a distance 's' above the bevelled rectangular patch on the same side. To minimize the potential interferences with the WLAN in addition to the WiMAX systems, a pair of L-shaped stubs ($w_L \times g_L$) is etched symmetrically at the upper edge of the ground plane as shown in Figure 1. The antenna of size 30 mm × 27 mm is printed on a substrate with relative permittivity 4.4, loss tangent 0.02 and thickness 1.6 mm. The proposed antenna structure is simulated using CST Microwave Studio.

3. ANTENNA DESIGN

3.1. Single Band-Notched UWB Monopole Antenna

A meander line resonator is etched in the radiating aperture of the planar UWB antenna to achieve single band-notched characteristic at WiMAX. The Z-shaped meandered structure and its parameters are shown in Figure 1(a). At 3.4 GHz (centre frequency of rejected WiMAX band — f_1), surface current on the meandered structure is shown in Figure 4. Since the spacing between the horizontal strips is small, current flows on the horizontal strips dominates more compared to that on the vertical strips and are in opposite phase between adjacent horizontal strips. Hence these currents do not contribute much to the radiation. The resonant frequency of a meander line is given by the expression $f_r = \frac{1}{2\pi\sqrt{LC}}$; where L and C are the equivalent inductance and capacitance of the meandered line. The values of L and C depend on the parameters of the meander line [19, 20].

Figure 5(a) and Figure 5(b) illustrate the effect of horizontal strip length (w_Z) and vertical strip length (l_Z) on S_{11} characteristics of the antenna respectively. It is observed that increasing either w_Z or l_Z decreases the notch frequency (WiMAX) because the inductance increases as the length of the strip increases. Another important parameter of a meander line is the strip width (w); narrow strip offers high inductance which in turn lowers the notch frequency again. Therefore, length of the strip required

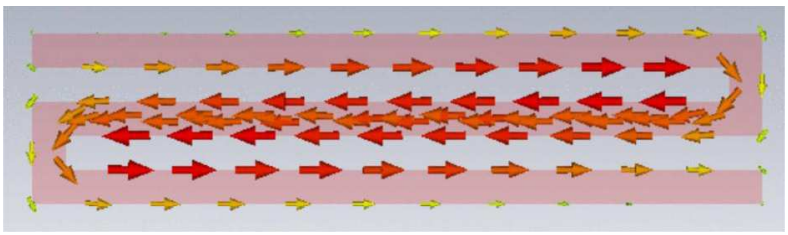

Figure 4. Simulated surface current distribution on Z-shaped parasitic element at 3.4 GHz.

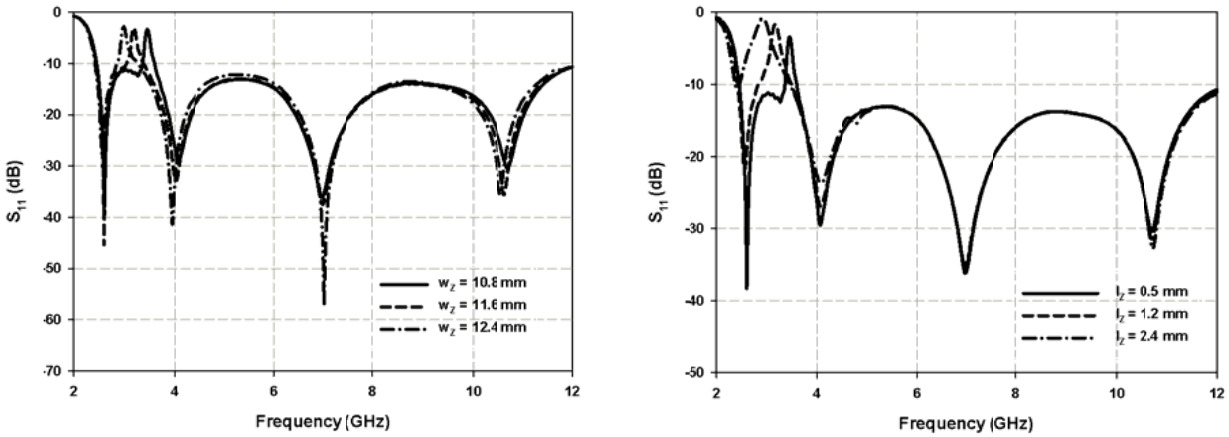

Figure 5. Effects of (a) horizontal strip length w_Z and (b) vertical strip length l_Z of Z-shaped parasitic on reflection coefficient of the single band-notched UWB antenna with all the other parameters same as in Figure 1.

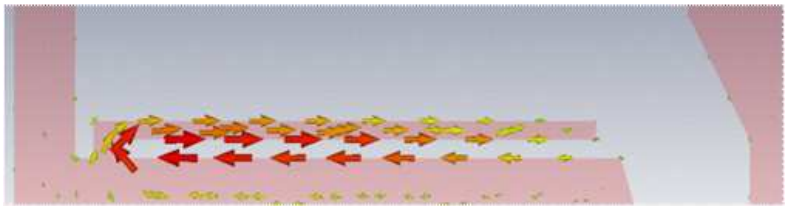

Figure 6. Simulated current distribution on L-shaped stub at 5.45 GHz.

to obtain a given notch frequency can be reduced by using narrow strips, which provides a compact notch structure for WiMAX band. Considering these factors the strip width (w) is chosen as 0.5 mm.

In Figure 5(b), a significant reduction in notched bandwidth is observed with decreasing l_Z. When l_Z decreases the spacing between the horizontal strips of the meandered structure also decreases. Thus the effective parallel-plate capacitance increases and results in narrowing of rejected bandwidth. From Figure 5(b), the required notch response is obtained for $l_Z = 0.5$ mm. After exhaustive simulation studies with $w = l_Z$, the length of the horizontal strip is given by an empirical expression: $w_Z = \frac{0.2\lambda_1}{\sqrt{\frac{\varepsilon_r+1}{2}}}$; where λ_1 is the free space wavelength at the designed notch frequency f_1. From Figure 5(a), it is found that the desired notch response at WiMAX is attained for $w_Z = 10.8$ mm.

3.2. Dual Band-Notched UWB Monopole Antenna

By employing a pair of symmetrical L-shaped stubs (to reject WLAN band) at the upper edge of the ground plane of the single band-notched antenna designed in the previous section, the proposed dual band-notched UWB antenna has been realised. At 5.45 GHz (centre frequency of rejected WLAN band — f_2), the surface current flows not only in the L-shaped stubs but also in the upper edge of the ground plane as shown in Figure 6. From the Figure 6, it is clear that the current present on the upper edge of the ground plane is actually the mirror image of that in the stubs, i.e., these two currents are in opposite phase. These currents do not contribute to the radiation, as done for the Z-shaped meandered structure. Here, the L-shaped stub acts as a quarter-wavelength resonator and its approximate length l_{LE} is given by the expression: $l_{LE} = \frac{0.25\lambda_2}{\sqrt{\frac{\varepsilon_r+1}{2}}}$; where $l_{LE} = (w_L - t) + g_L$, t is the thickness of the L-shaped stub ($t = 0.3$ mm) and λ_2 the free space wavelength at the notch frequency f_2.

Effects of horizontal strip length (w_L) and the gap (g_L) of the L-shaped stub on S_{11} are described in Figure 7(a) and Figure 7(b) respectively. In both the cases, as either w_L or g_L decreases, the notch frequency (WLAN) increases without disturbing the S_{11} characteristics of the single band-notched UWB antenna. Figure 7(b) reveals that the notched (WLAN) bandwidth is mainly determined by the parameter g_L which is actually the spacing between the horizontal strip of L-shaped stub and upper edge of the ground plane. Here, the notched bandwidth decreases as the parameter g_L decreases because of parallel-plate capacitance effect. Figure 7(a) and Figure 7(b) show that by choosing $g_L = 0.3\,\text{mm}$ and $w_L = 8.2\,\text{mm}$, the required notch response at WLAN band can be achieved. The simulated S_{11} confirm that Z-shaped meandered parasitic element and the L-shaped quarter wavelength stubs operate independently and have little effect on each other. Hence, offers great flexibility in the design of each notched band.

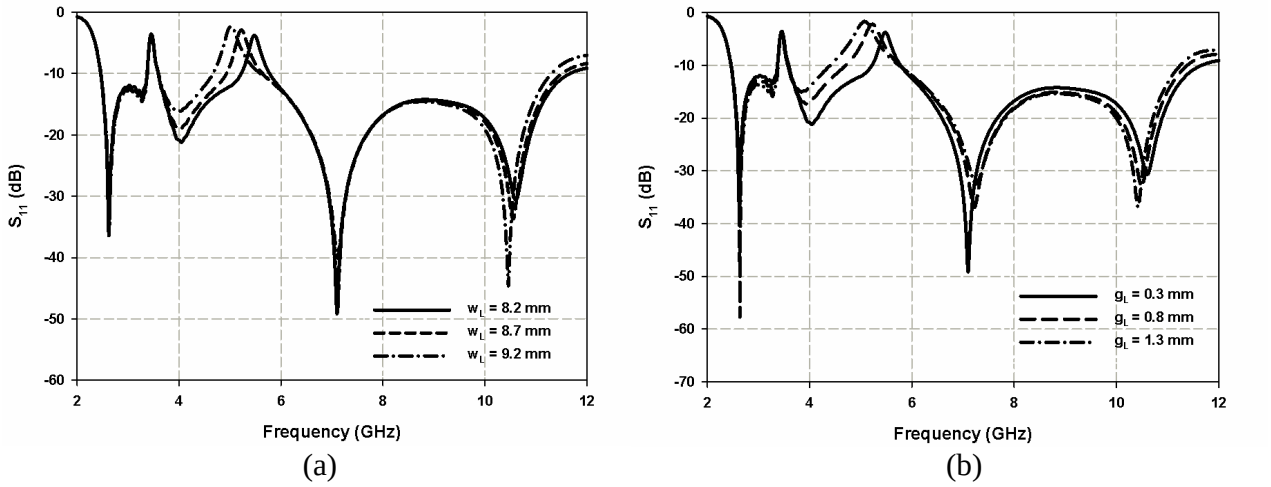

Figure 7. Effects of (a) horizontal strip length w_L and (b) gap g_L of L-shaped stub on reflection coefficient of the proposed antenna with all the other parameters same as in Figure 1.

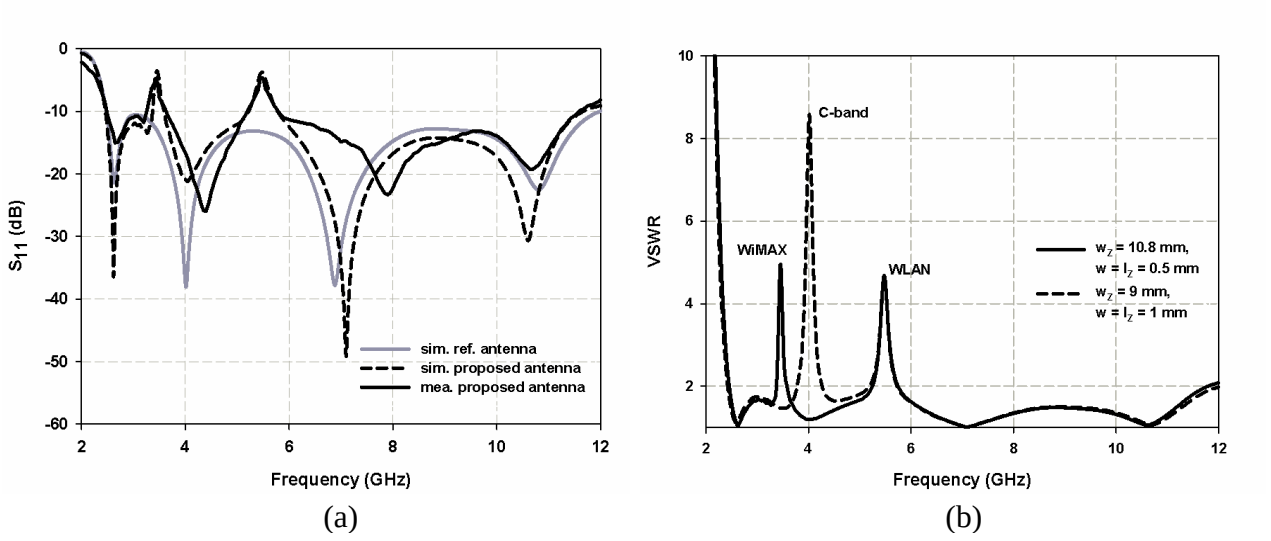

Figure 8. (a) Measured and simulated reflection coefficient of the proposed antenna. (b) Simulated VSWR of the proposed antenna with WiMAX/WLAN and C-band/WLAN notched bands (all the other parameters same as in Figure 1).

4. RESULTS AND DISCUSSIONS

The optimized dual band-notched antenna is fabricated, and S_{11} is measured using Rohde & Schwarz ZVB 20 vector network analyzer (10 MHz–20 GHz). The measured and simulated S_{11} of the proposed antenna along with the S_{11} of the reference antenna without notched functions are shown in Figure 8(a). A good agreement between these results is observed. The proposed antenna provides -10 dB S_{11} bandwidth from 2.5 to 11.5 GHz and successfully blocks out the WiMAX (3.3–3.6 GHz) and WLAN (5.2–5.75 GHz) bands. The simulated VSWR shown in Figure 8(b) indicates that the antenna can be used for the rejection of C-band (3.7–4.24 GHz) & WLAN combination also.

The measured radiation patterns of the antenna at 2.6 GHz, 4.4 GHz, 8 GHz and 10.5 GHz are shown in Figures 9(a)–(d). It can be seen that the antenna exhibits a nearly omni-directional and stable radiation patterns in the H-plane (xz-plane) over a wide frequency range. The E-plane (yz-plane) patterns are similar to 'figure-of-eight' like monopole antennas.

The simulated and measured peak gains of the antenna are provided in Figure 10. The gain is measured by gain comparison method, and it is observed, from the figure, that the proposed antenna exhibits a moderate gain response with variations less than 2.3 dB throughout the desired UWB frequency band except in the notched bands. Sharp decrease in gain at the notched bands ensures the band-rejection behaviour of the proposed antenna.

For short-range high-speed indoor UWB data communication, narrow pulse signals (such as

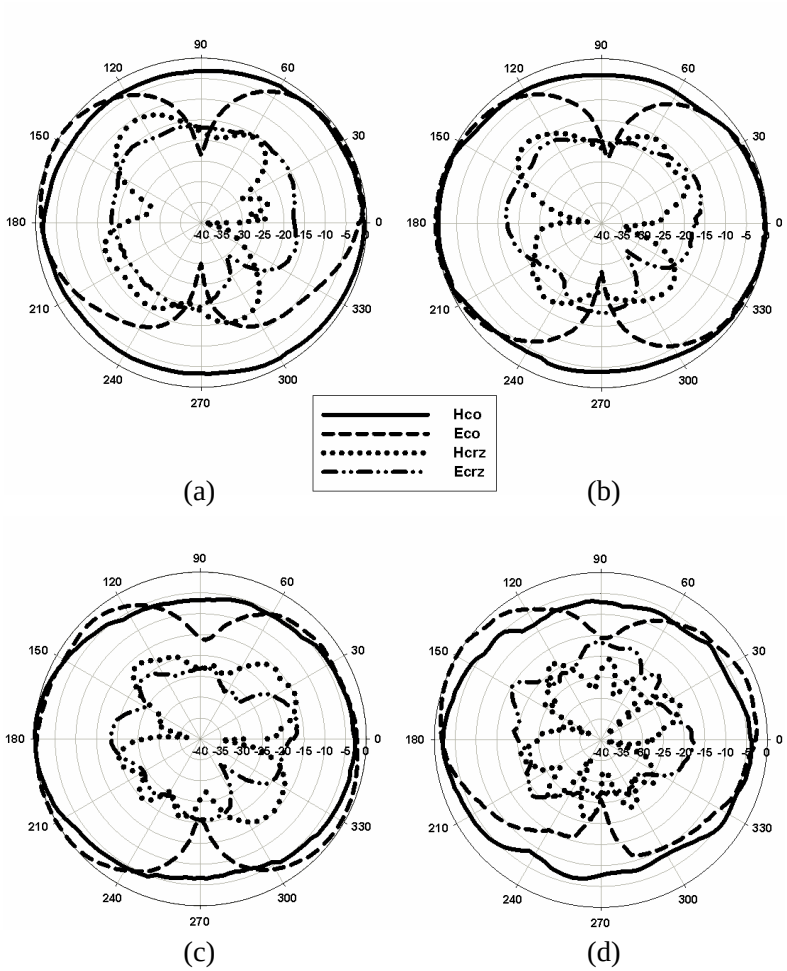

Figure 9. Measured radiation patterns at frequencies, (a) 2.6 GHz, (b) 4.4 GHz, (c) 8 GHz, and (d) 10.5 GHz.

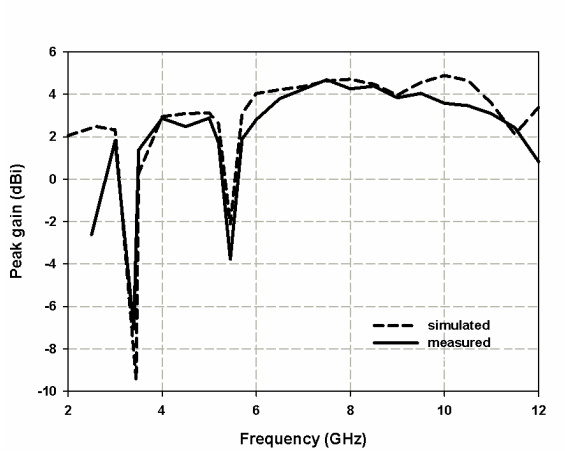

Figure 10. Measured and simulated peak gain of the proposed antenna.

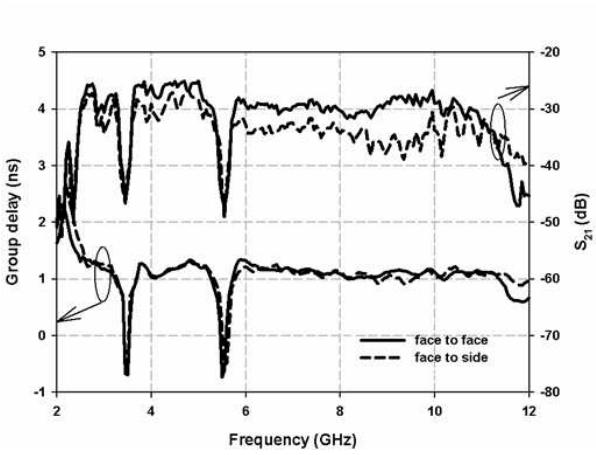

Figure 11. Measured overall transfer function (S_{21}) and group delay of the proposed antenna.

differentiated Gaussian pulse) are utilized for signal transmission and reception [21]. In the case of these systems, transfer function (S_{21}) and group delay are the most important parameters since it is a measure of dispersion behaviour of UWB antennas [22]. For ideal UWB applications, the magnitude of the antenna transfer functions and group delay should be as flat as possible in the operating band but drop drastically outside the band. The measurement system using vector network analyser comprises two identical dual band notched UWB antennas with one as transmitting and the other as receiving antenna with a separation of 25 cm [22, 23]. To study the antenna performance in different directions, measurements are taken in two different orientations, face to face and face to side. The measured overall transfer functions and group delays are described in Figure 11. For face to face orientation, S_{21} is moderately flat with variations less than 5 dB over the entire UWB band except in the notched bands (more than 15 dB) while for the face to side orientation it is almost similar to the result of face to face orientation with more variations from 8.5 to 10 GHz. For both the orientations, the variations in group delay for the proposed antenna is less than 0.5 ns across the UWB band except at two notched bands which indicates a linear phase response in the far field, thus minimises the pulse dispersion.

In order to study the time domain impulse response of the proposed antenna, both simulation (using CST) and measurement analyses are performed. For the analysis, a fourth-order Rayleigh pulse is used as the source pulse $S_i(t)$ since it can match the UWB band directly when the pulse width (τ) = 67 ps [21] and is generated numerically using the Expression (1).

$$S_i(t) = \left[\frac{16}{\tau^8}(t-1)^4 - \frac{48}{\tau^6}(t-1)^2 + \frac{12}{\tau^2}\right] \exp\left(-\left(\frac{t-1}{\tau}\right)^2\right) \tag{1}$$

The simulation configuration includes a transmitting antenna and several virtual probes located in the H-plane with the angles in steps of 45°. The normalised radiated pulses for two different locations of the virtual probe, i.e., at 0° and 90° are shown in Figure 12(a). In practical approach, the impulse responses are obtained mathematically by multiplying the spectra of the source pulse and the transmitting antenna transfer function (H_{TX}). An inverse Fourier transform is then applied to obtain the measured radiated pulse $S_r(t)$. The transfer functions of the transmitting (H_{TX}) and receiving (H_{RX}) antennas can be deduced from a simple measurement of the overall transfer function S_{21} in the frequency domain by using two identical antennas [23, 24]. The transfer function of transmitting and receiving antennas are given by (2) and (3).

$$H_{TX}(\omega, \theta, \varphi) = \sqrt{\frac{jS_{21}(\omega, \theta, \varphi)}{\lambda H_{CH}(\omega)}} \tag{2}$$

$$H_{RX}(\omega, \theta, \varphi) = \frac{\lambda H_{TX}(\omega, \theta, \varphi)}{j} \tag{3}$$

$$H_{CH}(\omega) = \frac{c}{2d\omega} \exp\left(\frac{-j\omega d}{c}\right) \tag{4}$$

where 'λ' is the free space wavelength, 'H_{CH}' the free space transfer function, 'c' the velocity of light in free space, and 'd' the distance between transmitting and receiving antennas.

Figure 12(a) illustrates the normalised source pulse, simulated and measured normalised radiated pulses in $+z$ direction and are shifted along the time axis to display clearly. It is observed that the radiated pulses in both the directions are nearly same which reveals that the proposed antenna has a stable omni-directional radiation pattern in the H-plane. Figure 12(b) compares the normalised power spectral density (PSD) of the radiated pulses with the FCC defined emission mask, which shows to what extent the spectra of the pulses are modified by the antenna. It is seen that the spectra of the simulated and measured radiated pulses maintain almost same shape as that of source pulse with two sharp decreases at 3.4 GHz and 5.45 GHz notched bands within the UWB band.

Moreover, the radiated spectrum completely complies with the stringent FCC's indoor emission mask in the frequency band of operation. Further, to evaluate the impulse response of the antenna quantitatively, another parameter called fidelity factor of the radiated pulses is calculated according to [25].

$$Fidelity = \max_{\tau_d} \left[\frac{\int_{-\infty}^{\infty} S_i(t) S_r(t+\tau_d)}{\sqrt{\int_{-\infty}^{\infty} S_i^2(t) \int_{-\infty}^{\infty} S_r^2(t)}} \right] \tag{5}$$

It is a measure of similarity between the source pulse and the radiated pulse, and the values obtained are given in Table 1. High fidelity factor (> 0.9) observed for angles ranging from 0° to 360° in H-plane

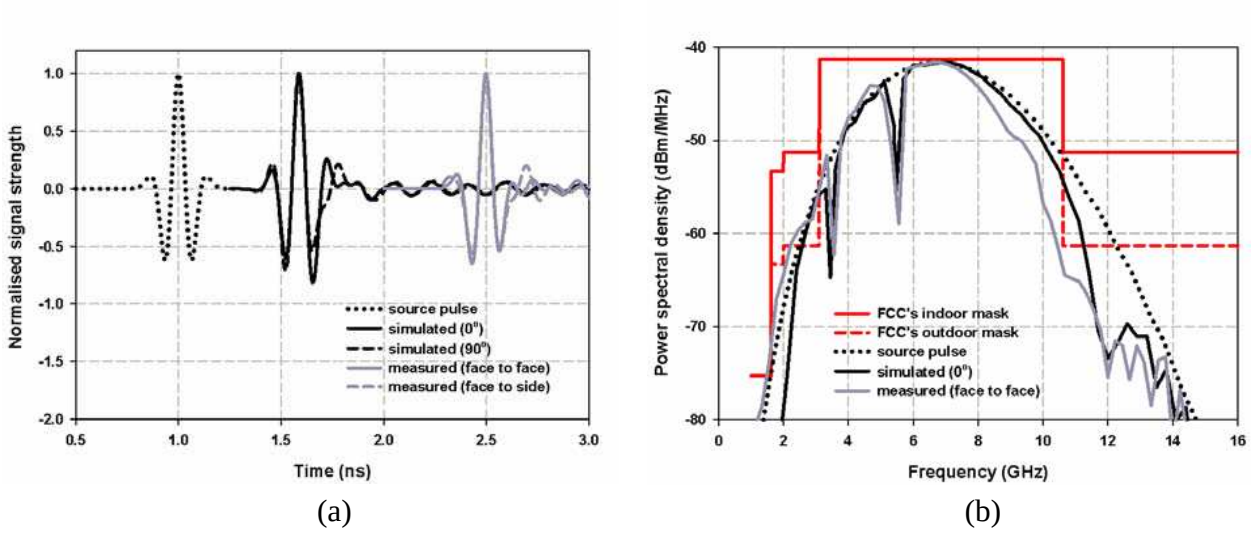

Figure 12. (a) Measured and simulated normalised radiated pulses for two different orientations. (b) Spectrum of source pulse and radiated pulses normalised to the FCC's indoor and outdoor emission masks.

Table 1. Measured and simulated fidelity factor for the proposed antenna in H-plane (xz-plane).

Angles	0° (face to face)	45°	90° (face to side)	135°	180°	225°	270°	315°	360°
Simulated	0.9719	0.9758	0.9483	0.9748	0.9733	0.9749	0.9478	0.9758	0.9719
Measured	0.9259	0.9281	0.9082	0.9349	0.9346	0.9278	0.9012	0.9206	0.9259

Table 2. Performance comparison of proposed antenna with the other structures reported.

Refs.	Overall size in λ_0 w.r.t. lower cut-off (mm)	Bandwidth (GHz)	Gain (outside notched band) (dBi)	G. delay (outside notched band) (ns)	Fidelity
[4]	$0.32 \times 0.32 \times 0.014$	2.75–11	2.0–5.0	< 1	-
[10]	$0.41 \times 0.31 \times 0.016$	3.1–10.6	2.5–6.0	< 2	0.73 – 0.95
[12]	$0.37 \times 0.28 \times 0.014$	2.8–11	2.5–7.0	< 2	-
[15]	$0.36 \times 0.40 \times 0.016$	3.15–11	3.7–6.5	< 1	-
Proposed	$0.25 \times 0.22 \times 0.013$	2.5–11.5	2.47–4.68	< 0.5	0.90–0.92

validates that the proposed antenna does not distort the source pulse significantly. Table 2 compares the results of the proposed antenna with other structures already reported. From the table it is clear that compared to other structures, the proposed antenna exhibits a superior performance in terms of gain (less variation), group delay and fidelity with a compact size. Based on the frequency domain and time domain analysis described, the proposed antenna has proved to be suitable for UWB communication.

5. CONCLUSION

By etching a Z-shaped meander line parasitic element and a pair of symmetric L-shaped quarter wavelength stubs an efficient dual band-notched UWB antenna is obtained, which avoid the interferences with co-existing WiMAX and WLAN bands respectively. An attractive merit of these notch structures is that the performances of these rejected bands can be controlled independently and easily by exploiting its inductance and capacitance properties, i.e., offers great flexibility in the notch design. Further, these notch structures have the advantage of occupying less space compared to the equivalent half-wavelength notch structures; hence promising candidates for miniaturized multiple band-notched antenna designs in future. The simulated refection coefficient is validated by experiment and reveals that the designed antenna has a broad bandwidth from 2.5 to 11.5 GHz with two controllable notched bands. The measured radiation patterns in the H-plane are nearly omnidirectional and stable over the entire operating bandwidth. The gain plot shows that the proposed antenna is very effective in rejecting the unwanted bands while maintaining a satisfactory response over the remaining operating bandwidth. Moreover, the measured group delay and fidelity reveal that the proposed antenna has an impressive impulse response, implying that it is an attractive candidate for various UWB applications.

REFERENCES

1. Chu, Q. X. and Y. Y. Yang, "A compact ultrawideband antenna with 3.4/5.5 GHz dual band-notched characteristics," *IEEE Trans. Antennas Propagation*, Vol. 56, No. 12, 3637–3644, 2008.
2. Nguyen, T. D., D. H. Lee, and H. C. Park, "Design and analysis of compact printed triple band-notched UWB antenna," *IEEE Antennas Wireless Propagation Letters*, Vol. 10, 403–406, 2011.
3. Zhang, S. M., F.-S. Zhang, W.-Z. Li, T. Quan, and H.-Y. Wu, "A compact UWB monopole antenna with WiMAX and WLAN band rejections," *Progress In Electromagnetics Research Letters*, Vol. 31, 159–168, 2012.
4. Sun, J. Q., X.-M. Zhang, Y.-B. Yang, R. Guan, and L. Jin, "Dual band-notched ultra-wideband planar monopole antenna with M- and W-slots," *Progress In Electromagnetics Research Letters*, Vol. 19, 1–8, 2010.
5. Chen, B., A. G. Wang, and G. H. Zhao, "Design of a novel ultrawideband antenna with dual band-notched characteristics," *Microwave and Optical Technology Letters*, Vol. 54, No. 10, 2401–2405, 2012.
6. Karimian, R., H. Oraizi, and S. Fakhte, "Design of a compact ultra-wide-band monopole antenna with band rejection characteristics," *IET Microw. Antennas Propag.*, Vol. 8, No. 8, 604–610, 2014.

7. Ryu, K. S. and A. A. Kishk, "UWB antenna with single or dual band notches for lower WLAN band and upper WLAN band," *IEEE Trans. Antennas Propagation*, Vol. 57, No. 12, 3942–3950, 2009.
8. Liu, W. X. and Y.-Z. Yin, "Dual band-notched antenna with the parasitic strip for UWB," *Progress In Electromagnetics Research Letters*, Vol. 25, 21–30, 2011.
9. Zhou, H. J., B. H. Sun, Q. Z. Liu, and J. Y. Deng, "Implementation and investigation of U-shaped aperture UWB antenna with dual band-notched characteristics," *Electronic Letters*, Vol. 44, No. 24, 1387–1388, 2008.
10. Gao, G. P., Z. L. Mei, and B. N. Li, "Novel circular slot UWB antenna with dual band-notched characteristic," *Progress In Electromagnetics Research C*, Vol. 15, 49–63, 2010.
11. Zhu, F., S. Gao, A. T. S. Ho, R. A. Abd-Alhameed, C. H. See, T. W. C. Brown, J. Li, G. Wei, and J. Xu, "Multiple band-notched UWB antenna with band-rejected elements integrated in the feed Line," *IEEE Trans. Antennas Propagation*, Vol. 61, No. 8, 3952–3958, Aug. 2013.
12. Liu, X., Y. Yin, P. Liu, J. Wang, and B. Xu, " A CPW-fed dual band-notched UWB antenna with a pair of bended dual-L-shape parasitic branches," *Progress In Electromagnetics Research*, Vol. 136, 623–634, 2013.
13. Ren, J. and Y. Yin, "A compact dual band-notched ultrawideband antenna with $\lambda/4$ stub and open slots," *Progress In Electromagnetics Research C*, Vol. 49, 133–139, 2014.
14. Wang, J., Y. Yin, X. Liu, and T. Wang, "Trapezoid UWB antenna with dual band-notched characteristics for WiMAX/WLAN bands," *Electronic Letters*, Vol. 49, No. 11, 685–686, 2013.
15. Mandal, T. and S. Das, "Design and analysis of a aoplanar waveguide fed Ultrawideband hexagonal open slot antenna with WLAN and WiMAX band rejection," *Microwave and Optical Technology Letters*, Vol. 56, No. 2, 434–442, 2014.
16. Wang, X., L. Wang, H. Zhou, and W. Lu, "Compact CPW-fed antenna with dual band-notched characteristics for UWB applications," *Microwave and Optical Technology Letters*, Vol. 56, No. 5, 1047–1049, 2014.
17. Coonrod, J. and B. Rautio, "Comparing microstrip and CPW performance," *Technical Feature, Microwave Journal*, 74–80, Jul. 2012.
18. Olaode, O. O., W. D. Palmer, and W. T. Joines, "Effects of meandering on dipole antenna resonant frequency," *IEEE Antennas and Wireless Propagation Letters*, Vol. 11, 122–126, 2012.
19. Tang, W. X., H. Zhao, X. Y. Zhou, J. Y. Chin, and T. J. Cui, "Negative index material composed of meander lines and SRRs," *Progress In Electromagnetics Research B*, Vol. 8, 103–114, 2008.
20. Booket, M. R., M. Kamyab, A. Jafargholi, and S. M. Mousavi, "Analytical modeling of the printed dipole antenna loaded with CRLH structures," *Progress In Electromagnetics Research B*, Vol. 20, 167–186, 2010.
21. Chen, Z. N., X. H. Wu, H. F. Li, N. Yang and M. Y. W. Chia, "Considerations for source pulses and antennas in UWB radio systems," *IEEE Trans. Antennas Propagation*, Vol. 52, No. 7, 1739–1748, 2004.
22. Bahadori, K. and Y. Rahmat-Samii, "A miniaturized elliptic-card UWB antenna with WLAN band rejection for wireless communications," *IEEE Trans. Antennas Propagation*, Vol. 55, No. 11, 3326–3332, 2007.
23. Klemm, M. and G. Troester, "Textile UWB antennas for wireless Body Area Networks," *IEEE Trans. Antennas Propagation*, Vol. 54, No. 11, 3192–3197, 2006.
24. Duroc, Y., A. Ghiotto, T. P. Vuong, and S. Tedjini, "UWB antennas: Systems with transfer function and impulse response," *IEEE Trans. Antennas Propagation*, Vol. 55, No. 5, 1449–1451, 2007.
25. Ma, T. G. and S. K. Jeng, "Planar miniature tapered-slot-fed annular slot antennas for ultrawideband radios," *IEEE Trans. Antennas Propagation*, Vol. 53, No. 3, 1194–1202, 2005.